**T. Beuselinck, C. Van Bavinchove,
Sazonov V.V., Chebukov S.Yu.**

Reconstruction of Spacecraft
Foton M-2 Attitude Motion by
Acceleration Measurements

T. Beuselinck, C. Van Bavinchove,
V.V. Sazonov, S.Yu. Chebukov

RECONSTRUCTION OF SPACECRAFT *FOTON M-2* ATTITUDE MOTION BY ACCELERATION MEASUREMENTS

Annotation

This preprint presents results of a reconstruction of the spacecraft *Foton M-2* attitude motion by measurements of the accelerometer TAS3. The *Foton M-2* attitude was already reconstructed by measurements of the Earth magnetic field and the angular rate. The TAS3 measurement data have been used for this purpose for the first time. These data contain secondary clear-cut component, which had unknown (three years ago) origin and made impossible their direct use for reconstruction of a spacecraft attitude motion. The secondary component proved to be caused by the Earth magnetic field. Understanding this fact allowed to introduce the proper correction of the TAS3 data into the processing procedure and to use them for the reconstruction. The given preprint contains descriptions of the improved procedure of processing TAS3 data and results of its testing and application. Testing consisted in the direct comparison of the motion reconstructed in a new way with the motion reconstructed by magnetic measurements. The new procedure allowed to reconstruct the real attitude motion of *Foton M-2* in the period 09.06.2005 — 14.06.2005 when magnetic measurements were not made.

Т. Бойзелинк, К. Ван Бавинхов, В.В. Сазонов, С.Ю. Чебуков. Определение вращательного движения спутника *Фотон М-2* **по данным измерений микроускорения.** Приведены результаты реконструкции неуправляемого вращательного движения спутника *Фотон М-2* по данным измерений акселерометра TAS-3. Вращательное движение этого спутника уже было найдено ранее по данным измерений магнитного поля Земли и угловой скорости. Данные TAS-3 использованы для этой цели впервые. Эти данные содержат четко выделяемую дополнительную составляющую, происхождение которой несколько лет назад было неизвестно и которая делала невозможным их прямое использование для реконструкции вращательного движения. Как выяснилось впоследствии, дополнительная составляющая вызвана влиянием магнитного поля Земли. Обнаружение этого факта позволило учесть при обработке данных TAS-3 необходимую поправку и использовать их для реконструкции вращательного движения *Фотона М-2*. В статье описывается модифицированный способ обработки данных TAS-3 и результаты его тестирования и применения. Тестирование состояло в прямом сравнении движения, реконструированного новым способом, с движением, построенным по магнитным измерениям. Новый способ позволил найти фактическое движение *Фотона М-2* в период 09.06.2005 — 14.06.2005, когда магнитные измерения не проводились.

1. Introduction. Starting from frequency properties, one can divide residual accelerations onboard the free flyers *Foton* in two parts: high-frequency and quasi-steady components. The high-frequency component is caused by elastic vibrations of a spacecraft body and by functioning onboard equipments. It has frequencies from above 1 Hz. The quasi-steady component is due to a spacecraft attitude motion as a rigid body, the gradient of the Earth gravitational field, and the atmosphere drag. Its spectrum lies within the range from 0 to 0.005 Hz.

Let us consider measurement data produced by a high-frequency accelerometer onboard a spacecraft. We suppose the accelerometer is precise enough so we can filter the correct quasi-steady component from its measurement data and clear away low frequencies from the high-frequency component. These two components have a different mechanical sense. The high-frequency component relates to the point, where the accelerometer is installed. It is very difficult and practically impossible to recalculate it for another point. On the contrary, the quasi-steady component contains, in principle, full information about a spacecraft motion as a motion of a rigid body.

There is a simple formula for calculation of quasi-steady accelerations along a given spacecraft motion. We remind it coupled with some definitions. Let a spacecraft be a rigid body moving along a low Earth orbit and let a point P be fixed with its frame. The difference between the gravitational field strength at point P and the absolute acceleration of this point is called a residual acceleration at point P. We denote the difference by $\mathbf{b}$. It plays a part of the gravitational acceleration $\mathbf{g}$ in orbital experiments in physics of fluids and material science. We assume that only the atmosphere drag is significant among nongravitational forces acting upon the spacecraft. Then $\mathbf{b}$ is defined by the formula [1]

$$\mathbf{b} = \mathbf{r} \times \dot{\boldsymbol{\omega}} + (\boldsymbol{\omega} \times \mathbf{r}) \times \boldsymbol{\omega} + \frac{\mu_e}{|\mathbf{R}|^3} \left[\frac{3 (\mathbf{R} \cdot \mathbf{r}) \mathbf{R}}{|\mathbf{R}|^2} - \mathbf{r} \right] + c\rho_a |\mathbf{v}| \mathbf{v} . \qquad (1)$$

Here, $\mathbf{r} = \overrightarrow{OP}$; the point O is the spacecraft center of mass; $\boldsymbol{\omega}$ is the absolute angular rate of the spacecraft; the dot above a symbol denotes differentiation with respect to time t; μ_e is the gravitational parameter of the Earth; $\mathbf{R}$ is the geocentric radius vector of point O; $\mathbf{v}$ is the velocity of point O with respect to the Earth surface; ρ_a is the atmosphere density at point O; c is the spacecraft ballistic coefficient.

If we reconstruct somehow a real spacecraft motion, we can calculate a real acceleration at point P by formula (1). This formula was derived for a general situation without any frequency restrictions. But for the *Foton* spacecraft it gives just a quasi-steady acceleration component. A spacecraft attitude motion can be reconstructed by processing measurement data from onboard sensors: magnetometers, angular rate sensors, accelerometers, etc.

The usual approach is as follows. Let we have measurement data from a sensor and the data cover a sufficiently long time interval of an uncontrolled

flight. First, we determine the real spacecraft attitude motion on that interval by statistical processing the measurement data. At that, we use spacecraft attitude motion equations, which are kinematic and dynamic equations of a rigid body. We find the solution of these equations that provides the best approximation of the measurement data. This solution is considered to be a reconstruction of the real motion. Then, we calculate along the solution the acceleration at any point of the spacecraft by formula (1).

We applied successfully this approach in the cases when a spacecraft attitude motion was reconstructed by Earth magnetic field measurements [2], angular rate measurements [3, 4], and acceleration measurements [4, 5]. This approach allowed us to process all measurements that were obtained in *Foton M-2* and were essential for analyzing quasi-steady accelerations excepting measurements of the high-frequency triaxial accelerometer TAS3. The TAS3 measurement data contain secondary clear-cut component, which had unknown (three years ago) origin and made impossible their direct use for reconstruction of a spacecraft attitude motion. The secondary component proved to be caused by the Earth magnetic field [6]. Understanding this fact allowed to introduce the proper correction of the TAS3 data into the processing procedure and to use them for the reconstruction. The given preprint contains descriptions of the improved procedure of processing TAS3 data and results of its testing and application. Testing consisted in the direct comparison of the motion reconstructed in a new way with the motion reconstructed by measurements of the Earth magnetic field. The new procedure allowed to reconstruct the real attitude motion of *Foton M-2* in the period $09.06.2005 - 14.06.2005$ when magnetic measurements were not made.

It may seem strange to reconstruct a spacecraft attitude motion by acceleration measurements. Magnetometers are better fit for this purpose. But there are at least two reasons that make such work of some use. First, we don't have another data. Second, we can use acceleration measurements for all kinds of testing: for testing measurement data in the low-frequency range, for testing spacecraft attitude motion equations, etc. These both reasons take place in the case of TAS3 data from *Foton M-2*.

2. Mathematical model of spacecraft attitude motion. The spacecraft is assumed to be an axially symmetric rigid body. To write equations of its motion and relations, used in processing measurement data, we introduce the following four right-hand Cartesian coordinate systems.

The system $Ox_1x_2x_3$ is fixed with the spacecraft body and is formed by its principal central axes of inertia. Point O is the spacecraft mass center; axis Ox_1 coincides with the spacecraft axis of symmetry and is directed from the capsule to the device unit. The spacecraft inertia tensor has the matrix $\text{diag}\,(I_1, I_2, I_2)$ in this system. We suppose that system $Ox_1x_2x_3$ is used for interpretation of measurement data implemented by various onboard sensors.

The auxiliary coordinate system $Oy_1y_2y_3$ serves for writing down the equations of spacecraft attitude motion. Axis Oy_1 coincides with axis Ox_1. Axes Ox_2 and Ox_3 are obtained from axes Oy_2 and Oy_3 by rotating system $Oy_1y_2y_3$ through the angle φ around axis Oy_1. To specify a kinematic relation between systems $Ox_1x_2x_3$ and $Oy_1y_2y_3$ we assume that absolute angular rate of the latter system has zero component along axis Oy_1. Let w_2, w_3 be components of this angular rate along axes Oy_2, Oy_3 and let the spacecraft absolute angular rate $\boldsymbol{\omega}$ have components $(\omega_1, \omega_2, \omega_3)$ in system $Ox_1x_2x_3$. Then $\dot{\varphi} = \omega_1$ and

$$\omega_2 = w_2 \cos\varphi + w_3 \sin\varphi\,, \quad \omega_3 = -w_2 \sin\varphi + w_3 \cos\varphi\,. \tag{2}$$

Greenwich system $CY_1Y_2Y_3$ is connected with the Earth. Its origin is in the Earth center; plane CY_1Y_2 coincides with the equator plane; axis CY_1 intersects the Greenwich meridian, the axis CY_3 is directed to the North Pole.

The quasi inertial system $CX_1X_2X_3$ serves for graphic representation of the spacecraft attitude motion. Axis CX_2 is directed along the vector $\mathbf{R} \times \dot{\mathbf{R}}$ at every instant; axis CX_3 lies in plane CY_1Y_2 and is directed to the ascending node of the spacecraft osculating orbit. The absolute value of the angular rate of this system did not exceed $5°$ per day.

We denote the transition matrix from system $Oy_1y_2y_3$ to Greenwich system by $\| a_{ij} \|_{i,j=1}^3$. Here, $a_{ij} = \cos(OY_i {}^\wedge Oy_j)$. The matrix elements are expressed as functions of the angles γ, δ, and β, which are defined in the following way. System $CY_1Y_2Y_3$ can be transformed to system $Oy_1y_2y_3$ by three sequential rotations (we suppose point O coincides with point C): (1) by angle $\delta + \pi/2$ around axis CY_2, (2) by angle β around new axis CY_3, (3) by angle γ around new axis CY_1, which coincides with axis Oy_1.

We specify the attitude of axis Oy_1 with respect to system $CX_1X_2X_3$ by the angles θ and ψ. Here, θ is the angle between axis Oy_1 and plane CX_1X_2; ψ is the angle between axis OX_1 and the projection of axis Oy_1 onto plane CX_1X_2. The unit vector of axis Oy_1 has the components $(\cos\theta \cos\psi, \cos\theta \sin\psi, -\sin\theta)$ in system $CX_1X_2X_3$. We use also another angle $\Lambda = \arccos(\cos\theta \sin\psi)$ between axes Ox_1 and CX_2.

The complete system of the spacecraft motion equations consists of two subsystems. The first subsystem describes the motion of point O; the second one describes the rotation of system $Oy_1y_2y_3$. The first subsystem is written in Greenwich coordinate system taking into account the real Earth gravitational field and the atmosphere drag. The field are represented by series in terms of solid spherical harmonics up to the order (16,16) inclusive. The atmosphere density are calculated according to model [7]. The solutions of the first subsystem were found from the condition of the best approximation of NORAD two line elements [2, 5].

The second subsystem consists of Poisson's kinematic equations for the first two rows of the matrix $\| a_{ij} \|$ as well as Euler's dynamic equations for the angular

rates w_2, w_3. We take into account four external torques in Euler's equations: gravitational and restoring aerodynamic ones, the torque from the Earth magnetic field, and the constant torque permanently directed along axis Ox_1. Calculating the aerodynamic torque, we assume the external envelope of the spacecraft is a sphere, its center being in axis Ox_1. Calculating the torque from the Earth magnetic field, we assume the own spacecraft dipole moment is parallel to axis Ox_1. The second subsystem has the form

$$\dot{w}_2 + \lambda\,\omega_1 w_3 = -\frac{3\mu_e}{R^5}(1-\lambda)y_1 y_3 + pE\rho_a vv_3 - mh'_3\,,$$

$$\dot{w}_3 - \lambda\,\omega_1 w_2 = \frac{3\mu_e}{R^5}(1-\lambda)y_1 y_2 - pE\rho_a vv_2 + mh'_2\,,$$

$$\dot{a}_{11} + w_2 a_{13} - w_3 a_{12} = \omega_e a_{21}\,, \tag{3}$$

$$\dot{a}_{12} + w_3 a_{11} = \omega_e a_{22}\,, \quad \dot{a}_{13} - w_2 a_{11} = \omega_e a_{23}\,,$$

$$\dot{a}_{21} + w_2 a_{23} - w_3 a_{22} = -\omega_e a_{11}\,,$$

$$\dot{a}_{22} + w_3 a_{21} = -\omega_e a_{12}\,, \quad \dot{a}_{23} - w_2 a_{21} = -\omega_e a_{13}\,,$$

$$\omega_1 = \Omega + \varepsilon(t-t_0)\,, \;\; \lambda = \frac{I_1}{I_2}\,, \;\; R = \sqrt{y_1^2 + y_2^2 + y_3^2}\,, \;\; v = \sqrt{v_1^2 + v_2^2 + v_3^2}\,.$$

Here, y_i, v_i, and h'_i are the components of the vectors $\mathbf{R}$, $\mathbf{v}$ (see Section 1), and $\mathbf{H}$, the Earth magnetic field strength at point O, in system $Oy_1y_2y_3$; the parameters p and m specify the aerodynamic and magnetic torques respectively; εI_1 is the constant torque along axis Ox_1; ω_e is the angular rate of the Earth rotation; E is the scale factor. We use in (3) the solution of Euler's equation $\dot{\omega}_1 = \varepsilon$ in the explicit form with the constant parameter Ω. A choice of the instant t_0 will be specified below.

We use 1000 s as a unit of time and 1000 km as a unit of length when numerical integrating equations (3). Then the units of the other quantities are following: $[v_i] = \text{km/s}$, $[\omega_i] = [w_i] = 10^{-3}\text{s}^{-1}$, $[p] = \text{cm/kg}$, $[h'_i] = 0.1\text{Oe}$, $[m] = 10^{-5}\text{Oe}^{-1}\text{s}^{-2}$, $[\varepsilon] = 10^{-6}\text{s}^{-2}$, $[\rho_a] = \text{kg/m}^3$, $E = 10^{10}$. The atmosphere density is calculated according to model [7]. The Earth magnetic field is calculated according to the analytical model IGRF2005. The third row of the transition matrix $\| a_{ij} \|$ is calculated at integration as a cross-product of its two first rows. We define a motion of system $Ox_1x_2x_3$ and functions $\omega_2(t)$, $\omega_3(t)$ for a solution of equations (3) by the relation $\varphi = \Omega(t-t_0) + \varepsilon(t-t_0)^2/2$ and formulas (2). The variables a_{1i} and a_{2i} are not independent owing to orthogonality of the matrix $\| a_{ij} \|$. On this reason, the initial values of a_{1i} and a_{2i} are expressed in terms of the angles γ, δ, and β.

The parameter λ in (3) is known: $\lambda = 0.27$. The parameters p, m, and ε are estimated by processing the measurement data along with initial values of a spacecraft attitude motion, i. e. they are fitted parameters.

Equations (3) and some other mathematical models in this preprint are simpler than analogous models used in [2] (nevertheless, we take into account the additional external torque produced by the Earth magnetic field). We did that to reduce the total number of fitted parameters and to avoid the use of a priori information and regularization techniques in statistical procedures. To compensate this simplification we content ourselves with processing of simple spacecraft motions when the component ω_1 of the angular rate is sufficiently large [2, 3].

3. The statistical technique of reconstruction of *Foton M-2* attitude motion by magnetic field measurements. Equations (3) were tested by using them in processing magnetic measurements made onboard *Foton M-2* and by comparing the results of this processing with results [2]. There was the equipment *Mirage* onboard *Foton M-2*. It measured the magnetic field inside the capsule during space experiments. That field was close to Earth's one and so we used equations (3) and *Mirage* measurements for reconstructing the attitude motion of the spacecraft by means of usual statistical techniques. We described briefly the technique used below (see details in [2]).

Magnetic field measurements, obtained in a time interval $t_0 \leq t \leq t_0 + T$ of several hours, were processed jointly. At first, we constructed the discrete Fourier series $\hat{h}_i(t)$ ($i = 1, 2, 3$) approximating components of the measured magnetic field in system $Ox_1x_2x_3$ in that interval. The root-mean-square errors of the approximation were usually less than 200γ ($1\gamma = 10^{-5}$ Oe). Then we calculated the numbers $t_n = t_0 + nT/N$, $h_i^{(n)} = \hat{h}_i(t_n)$, where $n = 0, 1, \ldots, N$. They served input information for searching a solution of equations (3) describing the real spacecraft motion in the interval $t_0 \leq t \leq t_0 + T$. We named the values $h_i^{(n)}$ by pseudo-measurements. There were usually $T = 100 - 300$ min, $T/N = 1$ min for *Foton M-2*.

Following the least squares method, we considered a solution of system (3) as reconstruction of the real spacecraft motion in the interval $t_0 \leq t \leq t_0 + T$ if it provided minimum to the functional [2]

$$\Phi = \sum_{i=1}^{3} \left\{ \sum_{n=0}^{N} \left[h_i^{(n)} - h_i(t_n) \right]^2 - (N+1)\Delta_i^2 \right\}, \tag{4}$$

$$h_i(t) = \sum_{j,k=1}^{3} H_j(t)a_{jk}(t), \quad \Delta_i = \frac{1}{N+1} \sum_{n=0}^{N} \left[h_i^{(n)} - h_i(t_n) \right].$$

Here, Δ_i are the estimates of constant biases in the pseudo-measurements $h_i^{(n)}$; $H_i(t)$ are the components of **H** (see Section 2) in Greenwich system. The quantities $H_i(t)$ were calculated using the model IGRF2005. We always used the initial point t_0 of the processed interval as the instant t_0 in (3). Functional (4) was minimized over 9 quantities: p, m, ε, Ω, $w_2(t_0)$, $w_3(t_0)$, $\gamma(t_0)$, $\delta(t_0)$, $\beta(t_0)$. The first

four quantities specify system (3), the other quantities specify its solution. We solved the minimization problem by Gauss–Newton's method.

We used appropriate standard deviations to characterize the accuracy of approximating the pseudo-measurements and scattering the fitted quantities. The standard deviations were calculated under the assumptions that errors in the pseudo-measurements $h_i^{(n)}$ were uncorrelated random variables with the same dispersion, errors in the pseudo-measurements with the same inferior index i had the same mean value (the quantities Δ_i in (4) are just the estimates of theses mean values).

The standard deviations were calculated in the following way. Let $\Phi_{\min}$ be the value of functional (4) at its minimum point, C be the matrix of Gauss–Newton's normal equations at that point ($2C$ is approximately equal to the matrix of the quadratic form $d^2\Phi$ at the minimum point of Φ). Then the standard deviation of errors in pseudo-measurements is estimated by the quantity

$$\sigma_H = \sqrt{\frac{\Phi_{\min}}{3N - 9}}.$$

The standard deviations of the fitted parameters are equal to the square roots of corresponding diagonal elements of the matrix $\sigma_H^2 C^{-1}$. We denote the standard deviations of the parameters p, m, and ε by σ_p, σ_m, and σ_ε.

4. Real attitude motion of *Foton M-2*. The technique above was applied for reconstructing the spacecraft motion in 6 time intervals. Some results are presented in Table 1 and in Figs. 1, 3 (we numbered figures according to episodes of motion rather than in the order of their citing in the text). The table contains certain characteristics of the intervals and the solutions of system (3) that approximate the motion. In particular, it contains the parameters p, m, ε and the standard deviations σ_H, σ_p, σ_m, σ_ε. The first column of the table contains (in brackets) the days of June 2005 that contains the respective interval. The figures are cited only for intervals 1, 4. They illustrate the accuracy of approximation of pseudo-measurements and the spacecraft attitude motion relative to system $CX_1X_2X_3$.

Each of Figs. 1, 3 are divided naturally into three parts — left-hand, middle and right-hand. The right-hand parts illustrate the quality of approximation of pseudo-measurements by the functions $h_i(t)$ defined in (4). Here, solid lines present plots of these functions on the interval $t_0 \leq t \leq t_0 + T$; marks indicate the points $\left(t_n, h_i^{(n)} - \Delta_i\right)$, $n = 0, 1, \ldots, N$. The middle parts of the figures contain the plots of the angular rates $\omega_i(t)$. There are two plots in each coordinate system. The plots, obtained by minimization of (4), are depicted by lines without marks. The left-hand sides of the figures contain the plots of time dependence of the angles Λ, θ, and ψ that represent the attitude of axis Ox_1 with respect to system $CX_1X_2X_3$. There are again two plots in each coordinate system. The

plots, obtained by minimization of (4), are depicted by lines without marks.

These examples demonstrate the worse accuracy of approximation of pseudo-measurements than it was obtained in [2] by using more complicated mathematical models. Here, the values of σ_H are about half as much again than in [2]. Nevertheless, the accuracy obtained is quite enough for our purposes. The standard deviations of initial angles $\gamma(t_0)$, $\delta(t_0)$, $\beta(t_0)$ are about $1.2°$ in the given examples; standard deviations of the angular rates $\Omega = \omega_1(t_0)$, $w_2(t_0) = \omega_2(t_0)$, $w_3(t_0) = \omega_3(t_0)$ are here about 0.002 deg./s. The mechanical interpretation of the found motion one can find in [2, 3].

5. The statistical technique of reconstruction of *Foton M-2* attitude motion by acceleration measurements. To reconstruct the spacecraft attitude motion by TAS3 measurement data we use at bottom the same technique as in Section 3. We take a time interval $t_0 \leq t \leq t_0 + T$ and, using low-frequency filtration of TAS3 data, construct in it the functions $B_i(t)$ ($i = 1, 2, 3$), which specify vector components of the quasi-steady acceleration in system $Ox_1x_2x_3$. These functions have the form of discrete Fourier series and contain the frequencies not more the 0.017 Hz [6]. We don't use the functions directly but deal with their values $t_n = t_0 + nT/N$, $B_i^{(n)} = B_i(t_n)$, $n = 0, 1, \ldots, N$. We refer to these values as the filtered data. TAS3 measurements have erroneous constant biases in each vector component. We changed on that reason the mean value of each function $B_i(t)$ in the interval $t_0 \leq t \leq t_0 + T$ to obtain zero mean value of filtered data $B_i^{(n)}$, $n = 0, 1, \ldots, N$.

Formula (1) gives the expressions for vector components of a quasi-steady acceleration in system $Ox_1x_2x_3$ in terms of variables of equations (3) and co-ordinates of point P. We would consider this point as a location of TAS3. But in fact, various TAS3 single-axis sensors have certain shifts with respect to each other. We suppose point P is the origin of the TAS3 own coordinate system and axes of that system are parallel to axes Ox_i ($i = 1, 2, 3$). We denote by $x_j^{(i)}$ the coordinates of the TAS3 sensor for axis Ox_i in the TAS3 coordinate system. Then we can write idealized calculation analogs for the functions $B_i(t)$ (with correct mean values) in the following form [6]

$$b_i = b_{ai} + \sum_{j=1}^{3} c_{ij} \left[x_j + x_j^{(i)} \right], \quad b_{ai} = c\rho_a v u_i \quad (i = 1, 2, 3), \qquad (5)$$

$$c_{11} = \omega_2^2 + \omega_3^2 + \frac{\mu_e}{R^3}(3\gamma_1^2 - 1), \quad c_{23} = \dot{\omega}_1 - \omega_2\omega_3 + \frac{3\mu_e}{R^3}\gamma_2\gamma_3,$$

$$c_{32} = -\dot{\omega}_1 - \omega_3\omega_2 + \frac{3\mu_e}{R^3}\gamma_3\gamma_2, \quad \text{etc.},$$

$$u_1 = v_1, \quad u_2 = v_2\cos\varphi + v_3\sin\varphi, \quad u_3 = v_3\cos\varphi - v_2\sin\varphi,$$

$$\gamma_1 = \frac{y_1}{R}, \quad \gamma_2 = \frac{y_2 \cos\varphi + y_3 \sin\varphi}{R}, \quad \gamma_3 = \frac{y_3 \cos\varphi - y_2 \sin\varphi}{R}.$$

Here, x_j are the coordinates of point P in system $Ox_1x_2x_3$; one has to use substitution of indices $1 \to 2 \to 3 \to 1$ in order to obtain the other c_{ij}.

The values of $x_j^{(i)}$ in mm are:

$$x_1^{(1)} = -56.2, \quad x_2^{(1)} = 48.5, \quad x_3^{(1)} = -57.0,$$
$$x_1^{(2)} = -36.5, \quad x_2^{(2)} = 22.3, \quad x_3^{(2)} = -70.5,$$
$$x_1^{(3)} = -31.0, \quad x_2^{(3)} = 48.5, \quad x_3^{(3)} = -27.8.$$

Formulas (5) don't take into account the influence of the Earth magnetic field on the TAS3 data as well as infra low-frequency errors in them. We mentioned this influence in Section 1 and we refer frequencies in the range $0 \div 0.0005\,\mathrm{Hz}$ to infra low-frequencies. We adopt models [6] for representation of these influence and errors and write out the relations:

$$B_i(t) \approx \Delta_{bi} + \hat{B}_i(t, \tau) \quad (i = 1, 2, 3),$$

$$\hat{B}_i(t, \tau) = b_i(t + \tau) + \sum_{j=1}^{3} m_{ij} h_j(t + \tau) + \chi_i(t), \tag{6}$$

$$\chi_i(t) = A_{i0}(t - t_0) + \sum_{k=1}^{K} A_{ik} \sin \frac{\pi k(t - t_0)}{T},$$

where Δ_{bi}, τ, m_{ij}, and A_{ik} are constant parameters; functions $b_i(t)$ and $h_i(t)$ (see (4)) are calculated along an appropriate solution of equations (3). As before, the initial point t_0 of the processed interval coincides with the instant t_0 in (3). The sense of some terms in (6) are following. The terms with $h_i(t)$ characterize the influence of the Earth magnetic field on the measurements; the terms $\Delta_{bi} + \chi_i(t)$ compensate infra low-frequency errors (including erroneous constant biases) in the measurements. The number K must not be large in order to the frequency $K/2T$ was below significant frequencies of functions (5).

We try to fit relations (6) by the least squares method and consider the functional

$$\Phi_b = \sum_{i=1}^{3} \left\{ \sum_{n=0}^{N} \left[B_i^{(n)} - \hat{B}_i(t_n, \tau) \right]^2 - (N+1)\Delta_{bi}^2 \right\}, \tag{7}$$

$$\Delta_{bi} = \frac{1}{N+1} \sum_{n=0}^{N} \left[B_i^{(n)} - \hat{B}_i(t_n, \tau) \right].$$

It is obtained by transformation of the standard functional of least squares method that arises at fitting relations (6) for the points $t = t_n$ $(n = 0, 1, \ldots, N)$ [4, 5]. We minimize the functional over initial conditions of a solution of equations (3) at the point t_0 and the parameters p, m, ε, τ, c, x_i, m_{ij}, A_{ik}. There are $26 + 3K$ parameters in aggregate.

We treat functional (7) in the following way. We join $25 + 3K$ of its arguments except τ in the vector z and consider (7) as the function $\Phi_b(z, \tau)$. The minimization of $\Phi_b(z, \tau)$ over z and τ is reduced to calculating the function

$$\hat{\Phi}_b(\tau) = \min_z \Phi_b(z, \tau)$$

at a sequence of points τ_n $(n = 1, 2, \ldots)$, which converges to the limit $\tau_* = \operatorname{argmin} \hat{\Phi}_b(\tau)$. We minimize $\Phi_b(z, \tau)$ over z, when τ was fixed, by Gauss–Newton's method. The quantities τ_* and $z_* = \operatorname{argmin} \Phi_b(z, \tau_*)$ are desired estimates of τ and z. We separate τ from the complete set of arguments of function (7) to simplify a preparation of the computer code for minimizing $\Phi_b(z, \tau)$. We took $\tau_1 = 0$ and used results of processing *Mirage* data in an appropriate time interval as an initial approximation to the minimum point of $\Phi_b(z, 0)$ in case of $\chi_i(t) \equiv 0$ $(i = 1, 2, 3)$. Then we passed to case of $\chi_i(t) \neq 0$, etc.

We used appropriate standard deviations to characterize the accuracy of the approximation of filtered data and scattering in the estimates τ_*, z_*. The standard deviation σ_b of errors in pseudo-measurements $B_i^{(n)}$ and the standard deviation σ_τ of τ_* were calculated by the formulas

$$\sigma_b = \sqrt{\frac{\hat{\Phi}_b(\tau_*)}{3N - 3K - 26}}, \quad \sigma_\tau^2 = 2\sigma_b^2 \left[\frac{\partial^2 \hat{\Phi}_b(\tau_*)}{\partial \tau^2} \right]^{-1}.$$

We evaluated the second derivative in the last formula by difference approximation.

Standard deviations of the components of z_* were calculated under assumption that $\tau = \tau_*$ was known exactly. Such standard deviations are called conditional ones. We found them in the following way. Let C be the matrix of normal equations, which appear at minimizing $\Phi_b(z, \tau_*)$ over z by Gauss-Newton's method; at that, C is calculated at the point z_* and $2C \approx \partial^2 \Phi_b(z_*, \tau_*)/\partial z^2$. Then the conditional standard deviations of the components of z_* are equal to the square roots of corresponding diagonal elements of the matrix $\sigma_b^2 C^{-1}$. We denote the conditional standard deviations of the quantities p, m, ε by σ_p, σ_m, σ_ε.

6. Real attitude motion of *Foton M-2* **(continuation).** The accelerometer TAS3 operated since 31.05.2005 till 14.06.2005. *Mirage* operated since 31.05.2005 till 09.06.2005. So we can reconstruct the spacecraft motion by two ways for time interval within the period $31.05 - 09.06$ and we can reconstruct the spacecraft motion in the remaining flight using TAS3 data.

11

An acceleration and a strength of a magnetic field have quite different physical nature. Therefore we compare measurement data of these quantities by comparing the spacecraft motions reconstructed in both ways above. This comparison was made for 6 time intervals listed in Table 1. Table 2 and Figs. $1 - 4$ contain the results of processing the acceleration data in those intervals at $K = 5$. Table 2 contains some fitted parameters minimizing functional (7) and appropriate standard deviations. The reconstructed motions in intervals 1, 4 are presented in figures. The plots with marks in left-hand and middle parts of Figs. 1, 3 describe the spacecraft attitude motion relative to system $CX_1X_2X_3$. These plots are defined at $\tau \leq t - t_0 \leq T + \tau$. One can compare the plots with marks and without them in the figures and feel that spacecraft motions, found in both above ways, coincide sufficiently well. The same precision of coincidence take place for the other intervals in Tables 1, 2.

Left-hand and right-hand parts of Figs. 2, 4 illustrate the accuracy of approximation of filtered data by their calculated analog. The left-hand parts contain the plots of functions $\Delta_{bi} + \hat{B}_i(t, \tau)$. They are depicted by solid lines. The marks near these plots show the filtered data $\left(t_n + \tau, B_i^{(n)}\right)$, $n = 0, 1, \ldots, N$. The right-hand parts of Figs. 2, 4 contain the plots of the residuals $e_i^{(n)} = B_i^{(n)} - \hat{B}_i(t_n, \tau) - \Delta_{bi}$ $(n = 0, 1, \ldots N; \;\; i = 1, 2, 3)$. These plots are the broken lines with vertexes in the points $\left(t_n + \tau, e_i^{(n)}\right)$. The standard deviation σ_b is a quantitative characteristic of the approximation accuracy. Its values are given in figure captions and in Table 2. These values are about the same as in [6], though we used there another way of constructing the calculated analog of functions $B_i(t)$. The figures and the values of σ_b in Table 2 demonstrate that correction for the magnetic field and elimination of infra low-frequency errors allow to fit rather exactly acceleration measurement data with their calculated analog.

Middle parts of Figs. 2, 4 contain the plots of the functions $b_i(t)$ (see (5)). These plots illustrate the level of quasi-steady accelerations nearby the TAS3 location in intervals 1 and 4.

Conditional standard deviations of the initial angles $\gamma(t_0)$, $\delta(t_0)$, $\beta(t_0)$ of found solutions don't exceed $1.5°$; conditional standard deviations of the corresponding quantities Ω, $w_2(t_0)$, $w_3(t_0)$ are less than 0.002 deg./s. These estimates are very close to the estimates obtained by processing *Mirage* measurements. The estimates of parameters p, m, ε and their standard deviations in Table 2 are about the same for each interval as in Table 1.

We can obtain some information about accuracy of our motion reconstruction comparing the estimates of c, τ, x_i, and m_{ij} found by the technique of Section 7 with analogous estimates found in a different way. The estimates of ballistic coefficient c in Table 2 are closed to the value 0.0016 m^2/kg that was obtained by processing trajectory measurements [2]. The estimates of x_i, τ, and m_{ij} in the table will be compared with the estimates obtained in [6] for the case when the

12

axes of the TAS3 own coordinate system were supposed to be parallel to the axes of system $Ox_1x_2x_3$. Let us begin with estimates of x_i. Their mean values were $x_1 = 21.5\,\text{mm}$, $x_2 = -87.5\,\text{mm}$, $x_3 = -234.1\,\text{mm}$. The standard deviations of the estimates of x_2 and x_3 were less than $1\,\text{mm}$, the standard deviations of the estimate of x_1 was about $5\,\text{mm}$. These estimates differ in a way from the estimates in Table 2. The difference of estimates for x_3 is especially large and stable; it is about $10\,\text{cm}$. The estimates of τ in Table 2 lies in the same range as estimates of this quantity in [6], but the have more large scattering. The estimates of m_{ij} in Table 2 have sufficiently small scattering which exceeds just slightly in the most cases the corresponding values of σ_{mij}. These estimates differ from estimates of the same quantities in [6] but are rather similar to them. The results of [6] are following (in units of Table 2): $m_{11} \approx -186$, $m_{12} \approx -100$, $m_{22} \approx -107$, $m_{33} \approx -177$ and $|m_{ij}| < 30$ for the other such coefficients.

Figs. $5 - 13$ and Table 3 present the results of reconstruction of the *Foton M-2* attitude motion after 09.06.2005 when *Mirage* didn't operate. All results were obtained at $K = 10$. We used method [4] to find initial approximation to the minimum point of $\Phi_b(z, 0)$ at $\chi_i(t) \equiv 0$. Figs. 6, 8, 10, 11, and 13 are analogous to Figs. 2, 4. Figs. 5, 7, 9, and 12 illustrate the the spacecraft motion and look like the left-hand and middle parts of Figs. 1, 3. Table 3 is similar to Table 2 but contains two additional columns with values of t_0 and T. Judging from the figures, the errors of motion reconstruction and measurement approximation in this series of time intervals are about the same as in the previous one. But comparing Tables 2 and 3 shows that the errors increased a little.

Conditional standard deviations of initial conditions of the found motions can be summarized as follows: the errors in the angles $\gamma(t_0)$, $\delta(t_0)$, $\beta(t_0)$ don't exceed $2.3°$; the errors in the angular rates Ω, $w_2(t_0)$, $w_3(t_0)$ are less than 0.0035 deg./s. The estimates of parameters p, m, etc. and their standard deviations in Table 3 look somewhat more scattered than in Table 2. Two large positive values of τ for intervals 10 and 13 seem to be anomalous. These two intervals supplied anomalous estimates of x_2, x_3, m_{23}, and m_{32}.

The jumps of τ at transitions from interval 11 to interval 12, and from interval 12 to interval 13 look anomalous too. Intervals 11 and 12 have the overlap with the length of 2 hours; intervals 12 and 13 have the overlap with the length of an hour. We reconstructed the motion in a few intermediate intervals within the sum of intervals 11, 12, and 13. Each intermediate interval had the length of 300 min. The time shift τ seemed to be a smooth function of t_0 for them. It is difficult to find the reason of this effect. It can consist in using a secondary minimum of functional (7), bugs in data, etc. But possible reasons are not so important. The calculated quasi-steady acceleration proved to be sufficiently close (see Figs. 10, 11, 13). Figs. 9, 12 illustrate the motion in the pairs of overlapping intervals. Each figure contains plots of the angles Λ, θ, ψ, and the angular rates ω_i for two solutions of equations (3). The conjunction of the solutions is not good in both

cases but one can feel some fluency of the reconstructed motion.

7. Conclusion. This preprint contains the results of processing measurement data produced by two different sensors onboard spacecraft *Foton M-2*. These sensors are the magnetometers of the equipment *Mirage* and the accelerometer TAS3. Measurement data of different kinds were processed separately by analogous statistical techniques based on the full system of the spacecraft attitude motion equations. The motions obtained by processing acceleration measurements were compared directly with the motions obtained by processing magnetic field measurements. The latter motions were considered as reference ones.

The correction of TAS3 measurement data for the Earth magnetic field and elimination of infra low-frequency errors allowed to achieve a good coincidence of spacecraft motions reconstructed in different ways. This good coincidence is not surprising because acceleration measurements contain some information about the Earth magnetic field in their additional low-frequency component. We have to note the favorable circumstance that frequencies of these additional components differ successfully from the motion frequencies. We have to note also a high accuracy of TAS3 acceleration measurements. If they are used in a proper manner then they give a sufficiently accurate reconstruction of the spacecraft attitude motion.

The use of correction TAS3 data for the Earth magnetic field allowed to reconstruct the real attitude motion of *Foton M-2* during the period 09.06.2005 — 14.06.2005, in which there were not magnetic measurements. It allowed to calculate real quasi-steady accelerations onboard the spacecraft at the time.

References

[1] V.V.Sazonov, M.M.Komarov, V.I.Polezhaev, S.A.Nikitin, M.K.Ermakov, V.M.Stazhkov, S.G.Zykov, S.B.Ryabukha, J.Acevedo, E.Liberman. Microaccelerations on board the Mir orbital station and prompt analysis of gravitational sensitivity of convective processes of heat and mass transfer. Cosmic research, 1999, vol. 37, No. 1, pp. 80-94.

[2] V.I.Abrashkin, N.L.Bogoyavlensky, K.E.Voronov, A.E.Kazakova, Yu.Ya.Puzin, V.V.Sazonov, N.D.Semkin, S.Yu.Chebukov. Uncontrolled motion of the Foton M-2 satellite and quasistatic microaccelerations on its board. Cosmic research, 2007, vol. 45, No. 5, pp. 424-444.

[3] V.I.Abrashkin, A.E.Kazakova, V.V.Sazonov, S.Yu.Chebukov. Determination of attitude motion of the Foton M-2 satellite using the data of onboard

measurements of its angular rate. Cosmic research, 2008, vol. 46, No. 2, pp. 146-165.

[4] V.V.Sazonov, S.Yu.Chebukov, V.I.Abrashkin, A.E.Kazakova, A.S.Zaitsev. Analysis of low-frequency microaccelerations onboard the Foton-11 satellite. Cosmic research, 2001, vol. 39, No. 4, pp. 391-407.

[5] V.V.Sazonov, S.Yu.Chebukov, V.I.Abrashkin, A.E.Kazakova, A.S.Zaitsev. Low-frequency microaccelerations onboard the Foton-11 satellite. Cosmic research, 2004, vol. 42, No. 2, pp. 178-193.

[6] T.Beuselinck, C.Van Bavinchove, V.V.Sazonov, S.Yu.Chebukov. Analysis of quasi-steady component in acceleration measurement data obtaind onboard Foton M-2. Preprint of KIAM, No. 8, 2008.

[7] GOST R (State standard) 25645.166-2004. Earth upper atmosphere. Density model for ballistic support of flights of artificial Earth satellites. Moscow, 2004.

Table 1. Results of processing magnetic field measurements onboard *Foton M-2*.

Interval (date)	t_0 UTC	T (min)	s_H (g)	p 10^{-5}m/kg	s_p	m 10^{-7}Oe^{-1}s^{-2}	s_m	e 10^{-8}s^{-2}	s_e
1 (4)	13:15:06	270.3	1334	–16.1	0.61	–0.18	0.35	2.30	0.047
2 (5)	10:36:15	270.3	1991	–3.60	1.4	1.87	0.48	0.557	0.054
3 (6)	11:17:34	270.2	1763	–20.6	0.84	1.49	0.37	2.53	0.040
4 (7)	09:18:45	270.2	1966	–14.3	1.4	6.78	0.36	0.241	0.044
5 (8)	09:20:02	270.2	2143	–8.33	1.5	5.11	0.43	0.061	0.044
6 (9)	09:21:20	270.2	2342	–4.79	1.7	4.53	0.44	0.088	0.049

Table 2. Estimates of adjusting parameters for the accelerometer TAS3. The unit of m_{ij} and s_{mij} is 10^{-7} m/(s$^2\cdot$Oe).

Interval	s_b (10^{-6} m/s^2)	t (s)	s_t (s)	p (10^{-5} m/kg)	s_p	m (10^{-7} Oe^{-1}s^{-2})	s_m	e (10^{-8} s^{-2})	s_e	c (10^{-3} m^2/kg)	s_c
1	0.896	−44.5	6.7	−14.3	1.0	1.08	0.54	2.58	0.061	1.734	0.029
2	0.848	−46.9	6.4	−8.21	1.1	3.72	0.42	0.754	0.040	1.948	0.026
3	0.837	−7.3	6.6	−18.5	0.96	1.18	0.45	2.49	0.031	1.707	0.025
4	0.871	−14.0	6.7	−13.1	0.99	6.57	0.42	0.421	0.034	1.915	0.026
5	0.950	−20.6	7.5	−9.98	1.2	4.16	0.47	0.312	0.038	1.733	0.028
6	0.989	2.3	7.6	−6.40	1.2	3.85	0.47	0.190	0.041	1.619	0.032

Interval	x_1 (mm)	s_{x1} (mm)	x_2 (mm)	s_{x2} (mm)	x_3 (mm)	s_{x3} (mm)	m_{11}	s_{m11}	m_{12}	s_{m12}	m_{13}	s_{m13}
1	−29.2	3.9	−42.9	5.8	−310.4	1.6	−198.8	3.0	−19.3	3.2	−98.5	2.4
2	−37.4	3.5	−54.6	5.0	−320.1	1.5	−207.4	2.7	−12.9	2.2	−99.2	2.3
3	−26.5	3.2	−33.1	5.5	−331.8	1.4	−214.7	2.8	−14.4	2.2	−96.3	2.3
4	−60.8	4,0	−46.9	6.2	−353.4	2.0	−210.4	3.7	−8.9	2.0	−75.9	2.1
5	−49.5	4.8	−74.5	7.7	−366.3	3.0	−221.2	3.5	−20.3	2.3	−83.0	2.5
6	−59.5	5.1	−55.0	9.0	−377.4	3.3	−237.1	3.6	−13.3	2.6	−86.0	2.6

Interval	m_{21}	s_{m21}	m_{22}	s_{m22}	m_{23}	s_{m23}	m_{31}	s_{m31}	m_{32}	s_{m32}	m_{33}	s_{m33}
1	4.2	2.7	−112.0	1.6	−19.3	2.2	−28.6	2.7	−27.4	2,3	−165.8	1.7
2	4.7	2.6	−107.3	1.6	−20.1	2.0	−9.4	2.6	−22.0	2.6	−168.6	1.7
3	3.7	2.6	−105.1	1.6	−28.6	2.1	−21.8	2.6	−5.2	2.7	−168.5	1.6
4	8.6	3.5	−109.2	1.6	−26.7	2.1	−27.1	3.5	−10.3	2.6	−168.9	1.7
5	5.6	3.2	−107.5	1.8	−24.9	2.4	−11.7	3.3	−20.1	3.0	−164.8	1.9
6	7.4	3.3	−105.2	1.8	−21.0	2.6	−9.7	3.3	−20.1	3.4	−164.9	2.0

Table 3. Estimates of adjusting parameters for the accelerometer TAS3. The unit of m_{ij} and s_{mij} is 10^{-7} m/(s²·Oe).

Interval (date)	t_0 UTC	T (min)	s_b (10^{-6} m/s²)	t (s)	s_t (s)	p (10^{-5} m/kg)	s_p	m (10^{-7} Oe⁻¹s⁻²)	s_m (Oe⁻¹s⁻²)	e (10^{-8} s⁻²)	s_e (s⁻²)	c (10^{-3} m²/kg)	s_c (m²/kg)
7(10)	08:00:00	299.0	1.060	–5.0	9.5	–29.4	1.4	–4.98	0.78	2.15	0.033	1.589	0.034
8(11)	09:30:00	303.0	0.980	–39.9	6.2	–7.18	1.1	5.20	0.38	–0.859	0.026	1.635	0.032
9(12)	09:30:00	303.5	1.135	–61.2	8.0	–1.12	1.1	2.68	0.49	–1.35	0.032	1.495	0.029
10(13)	08:30:00	303.5	1.456	127.2	8.6	–24.2	1.3	15.0	0.54	2.74	0.042	2.364	0.039
11(14)	08:30:00	303.5	1.390	–84.8	11.7	–4.62	1.3	–2.80	0.84	–0.370	0.041	1.300	0.034
12(14)	11:30:00	303.5	1.495	–3.4	10.4	–30.8	1.3	–16.3	1.00	2.16	0.037	1.154	0.038
13(14)	15:30:00	303.5	1.446	216.5	9.6	–24.1	1.4	15.5	0.59	2.81	0.035	1.267	0.040

Interval	x_1 (mm)	s_{x1} (mm)	x_2 (mm)	s_{x2} (mm)	x_3 (mm)	s_{x3} (mm)	m_{11}	s_{m11}	m_{12}	s_{m12}	m_{13}	s_{m13}
7	–12.1	4.7	–24.9	8.6	–349.3	2.9	–235.1	3.4	–16.4	3.3	–120.9	3.5
8	–69.8	4.2	–77.4	7.9	–372.5	3.0	–239.4	3.0	–23.3	2.3	–84.3	2.2
9	–44.5	4.6	–68.6	8.4	–358.9	3.3	–231.9	3.4	–24.3	2.9	–97.1	2.6
10	–34.3	6.6	19.0	10.4	–434.9	5.1	–205.7	3.6	–18.6	3.4	–91.1	3.8
11	–22.5	5.3	–69.5	11.6	–389.2	4.5	–226.1	3.9	–21.8	4.4	–130.7	4.2
12	–8.2	5.6	–45.1	13.5	–390.6	4.6	–200.0	3.2	–25.3	5.3	–149.3	4.7
13	–22.1	5.7	41.3	14.3	–438.8	4.4	–196.9	2.6	–13.8	3.8	–96.8	3.7

Interval	m_{21}	s_{m21}	m_{22}	s_{m22}	m_{23}	s_{m23}	m_{31}	s_{m31}	m_{32}	s_{m32}	m_{33}	s_{m33}
7	13.6	3.3	–97.8	2.0	–23.0	2.7	–21.0	3.3	–10.9	3.6	–157.5	2.1
8	6.8	2.7	–105.8	1.6	–19.4	2.4	–24.6	2.7	–23.4	3.2	–161.5	1.9
9	7.2	3.1	–100.8	1.9	–16.7	2.6	–15.3	3.1	–25.9	3.3	–154.2	2.1
10	11.4	3.3	–101.9	2.6	–38.1	3.0	–19.2	3.3	2.9	3.5	–160.2	2.7
11	15.0	3.5	–102.0	2.5	–22.4	3.4	–19.6	3.5	–21.7	4.5	–157.9	2.7
12	9.6	3.0	–105.6	2.7	–27.1	4.0	–22.0	3.0	–11.7	5.4	–163.4	2.8
13	9.0	2.5	–95.7	2.6	–48.1	3.6	–7.6	2.5	21.9	5.1	–161.3	1.4
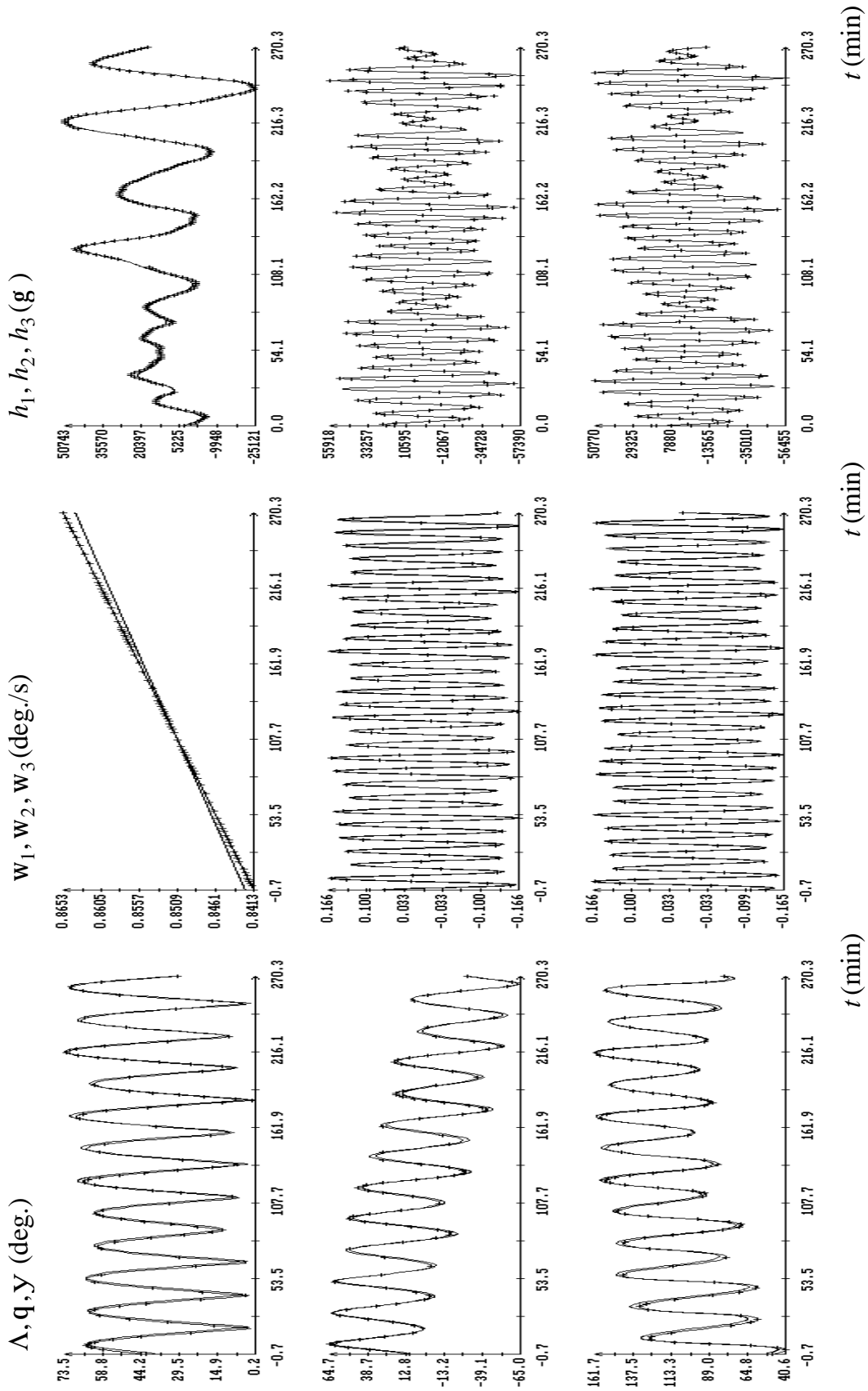
Fig. 1. The motion in interval 1. The instant $t = 0$ corresponds to 13:15:06 UTC 04.06.2005, $s_H = 1334\,\text{g}$.

19
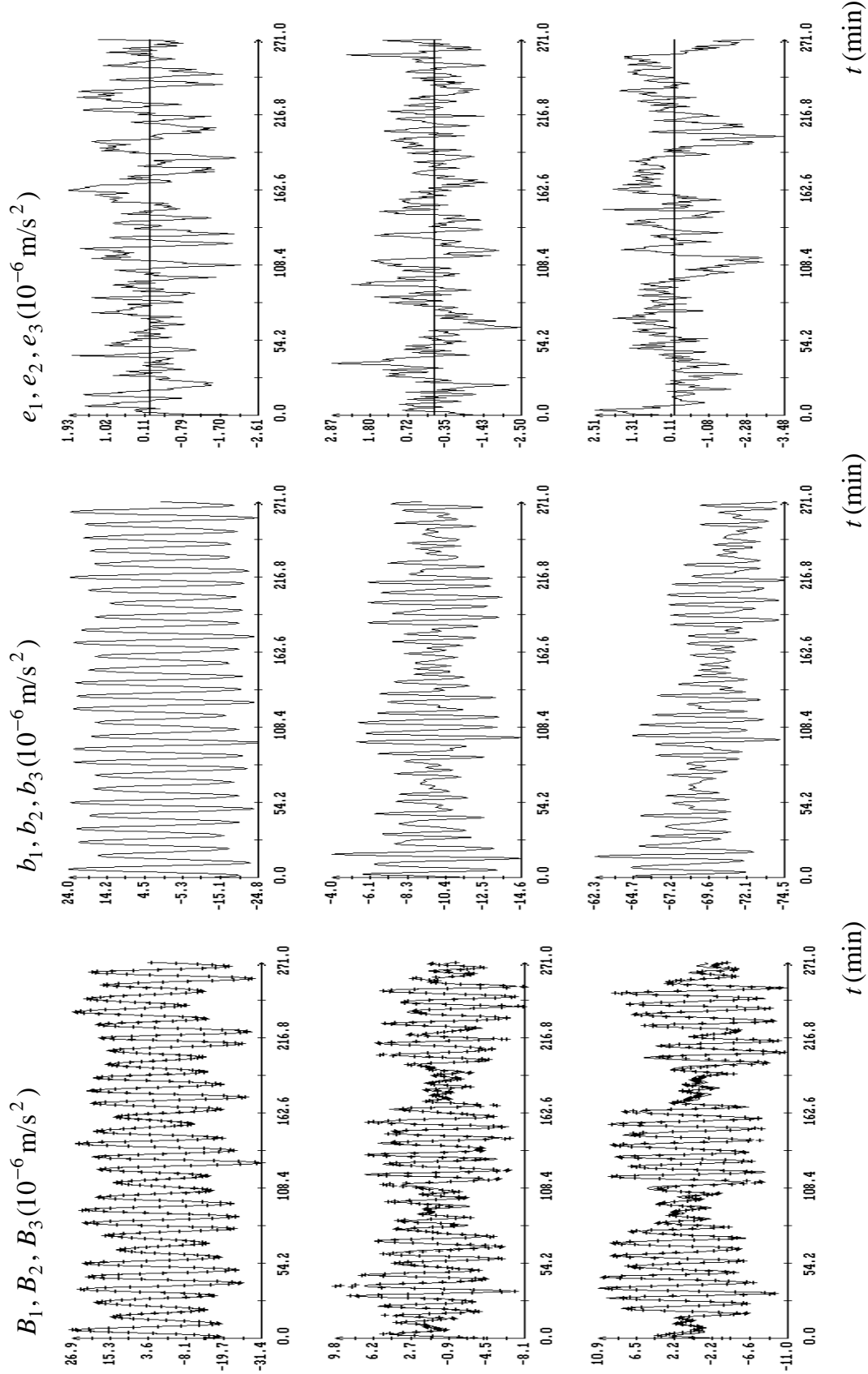
Fig. 2. The acceleration in interval 1. The instant $t = 0$ corresponds to $t_0 + \mathrm{t}$, $t_0 = 13{:}15{:}06$ UTC 04.06.2005, $\mathrm{t} = -44.5\,\mathrm{s}$, $\mathrm{s_t} = 6.7\,\mathrm{s}$, $\mathrm{s}_b = 0.896 \cdot 10^{-6}\,\mathrm{m/s}^2$.
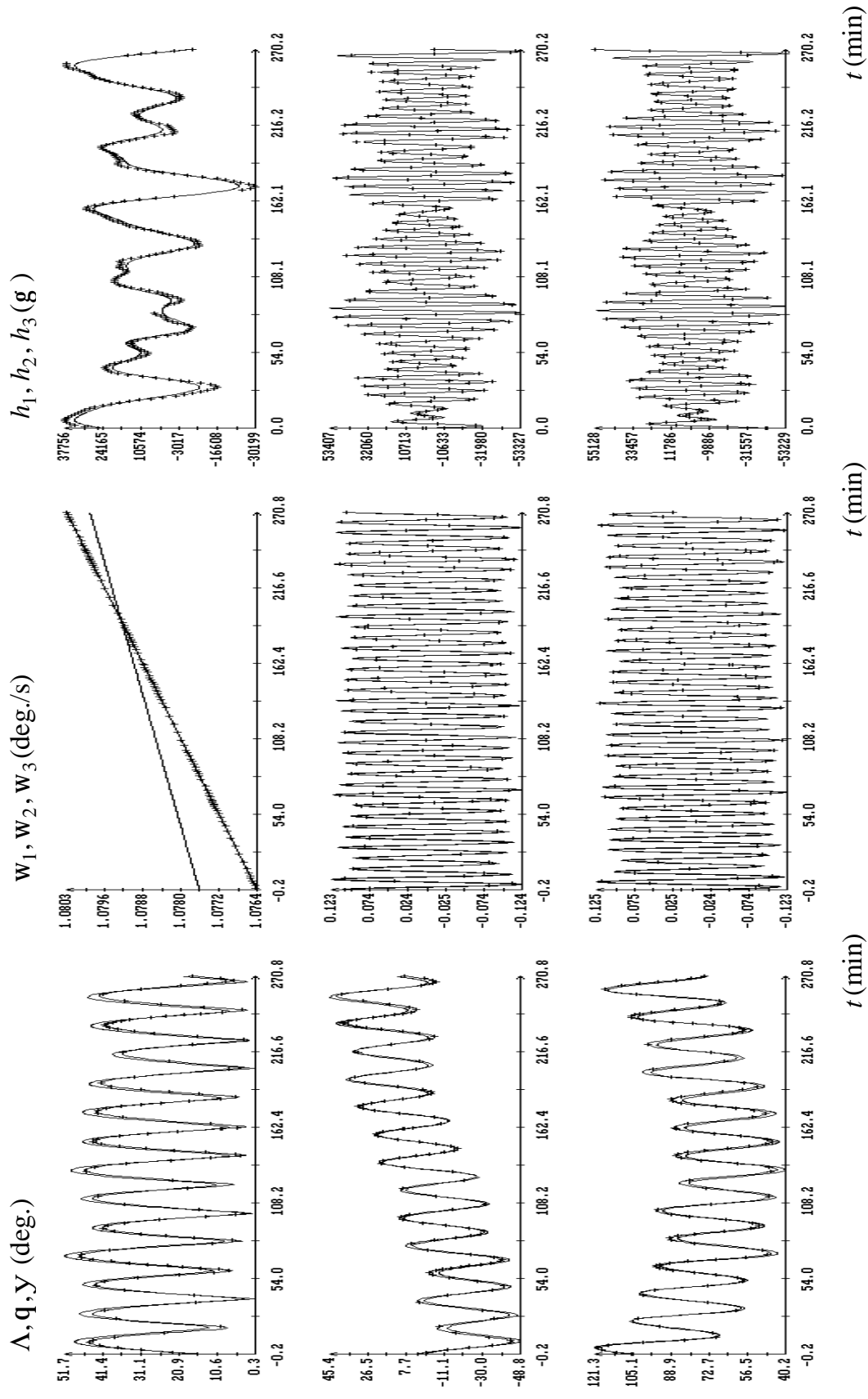
Fig. 3. The motion in interval 4. The instant $t = 0$ corresponds to 09:18:45 UTC 07.06.2005, $s_H = 1966\,\mathrm{g}$.
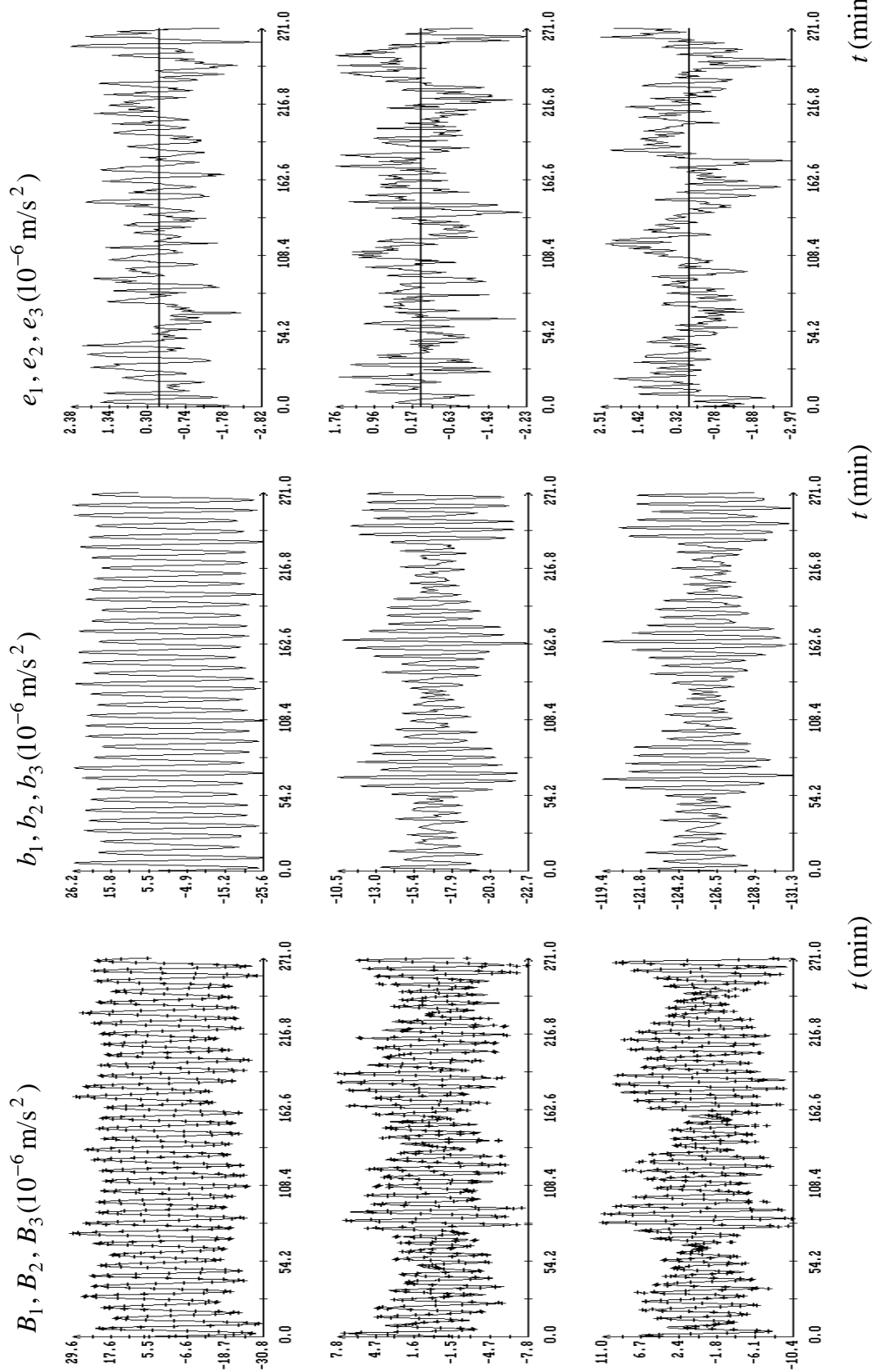
Fig. 4. The acceleration in interval 4. The instant $t = 0$ corresponds to $t_0 + \mathsf{t}$, $t_0 = $ 09:18:45 UTC 07.06.2005, $\mathsf{t} = -14.0\,\mathrm{s}$, $\mathsf{s_t} = 6.7\,\mathrm{s}$, $\mathsf{s}_b = 0.871 \cdot 10^{-6}\,\mathrm{m/s}^2$.
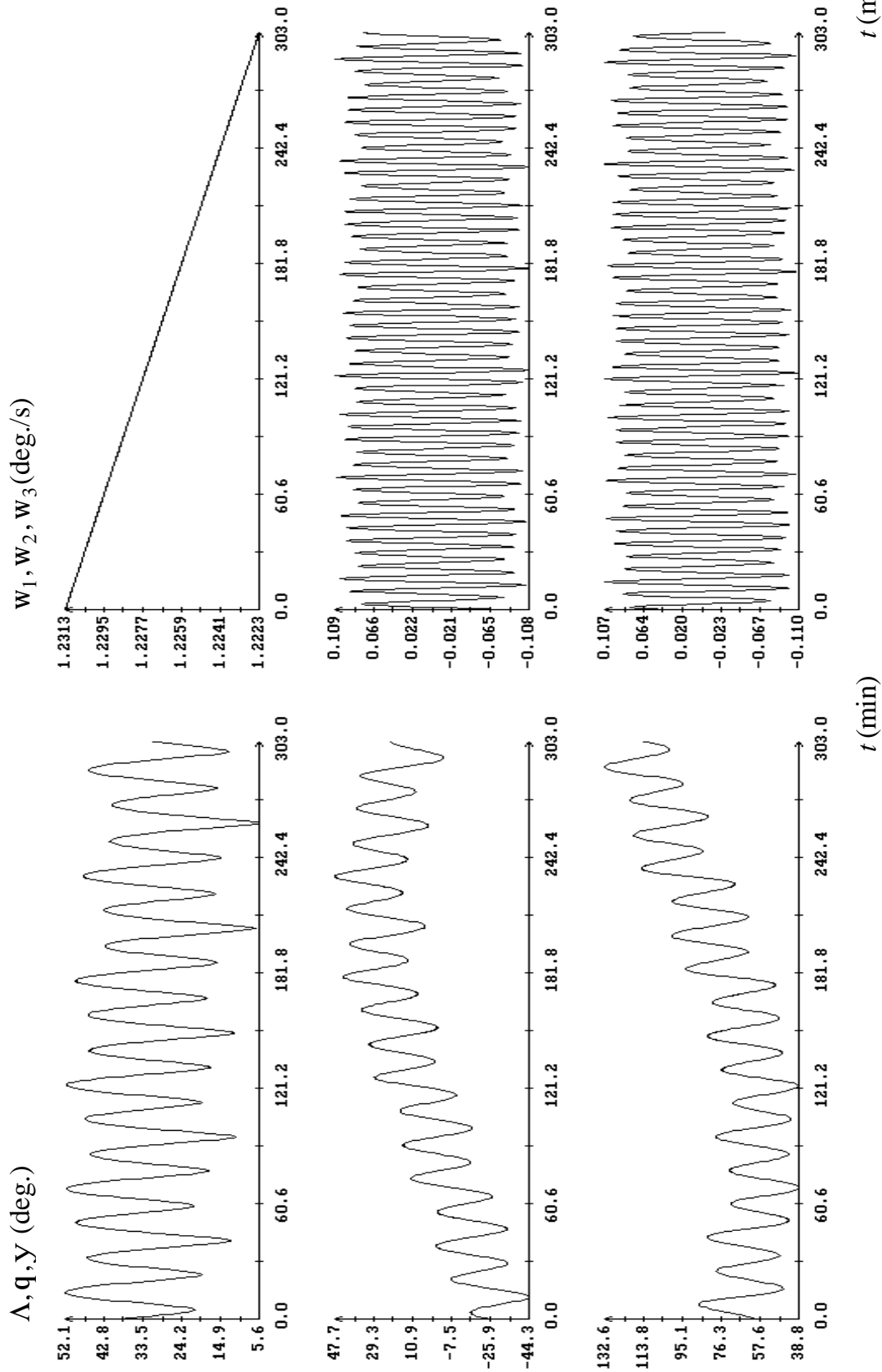
Fig. 5. The motion in interval 8. The instant $t = 0$ corresponds to $t_0 + t$, $t_0 = 09{:}30{:}00$ UTC 11.06.2005, $t = -39.9\,s$, $s_t = 6.2\,s$, $s_b = 0.980 \cdot 10^{-6}\,m/s^2$.
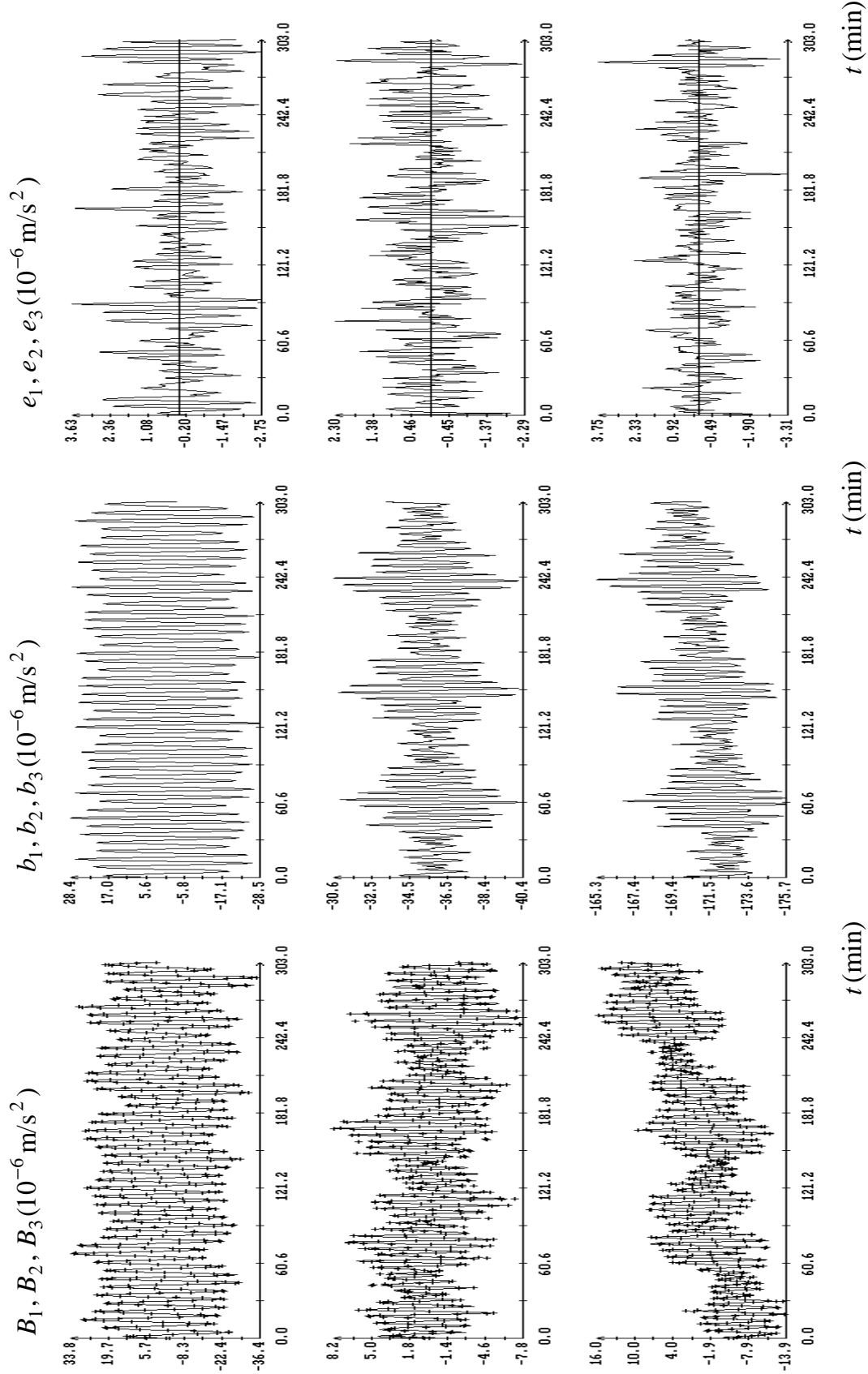
Fig. 6. The acceleration in interval 8. The instant $t = 0$ corresponds to $t_0 + \mathsf{t}$, $t_0 = 09{:}30{:}00$ UTC 11.06.2005, $\mathsf{t} = -39.9\,\mathrm{s}$, $\mathsf{s_t} = 6.2\,\mathrm{s}$, $\mathsf{s}_b = 0.980 \cdot 10^{-6}\,\mathrm{m/s}^2$.
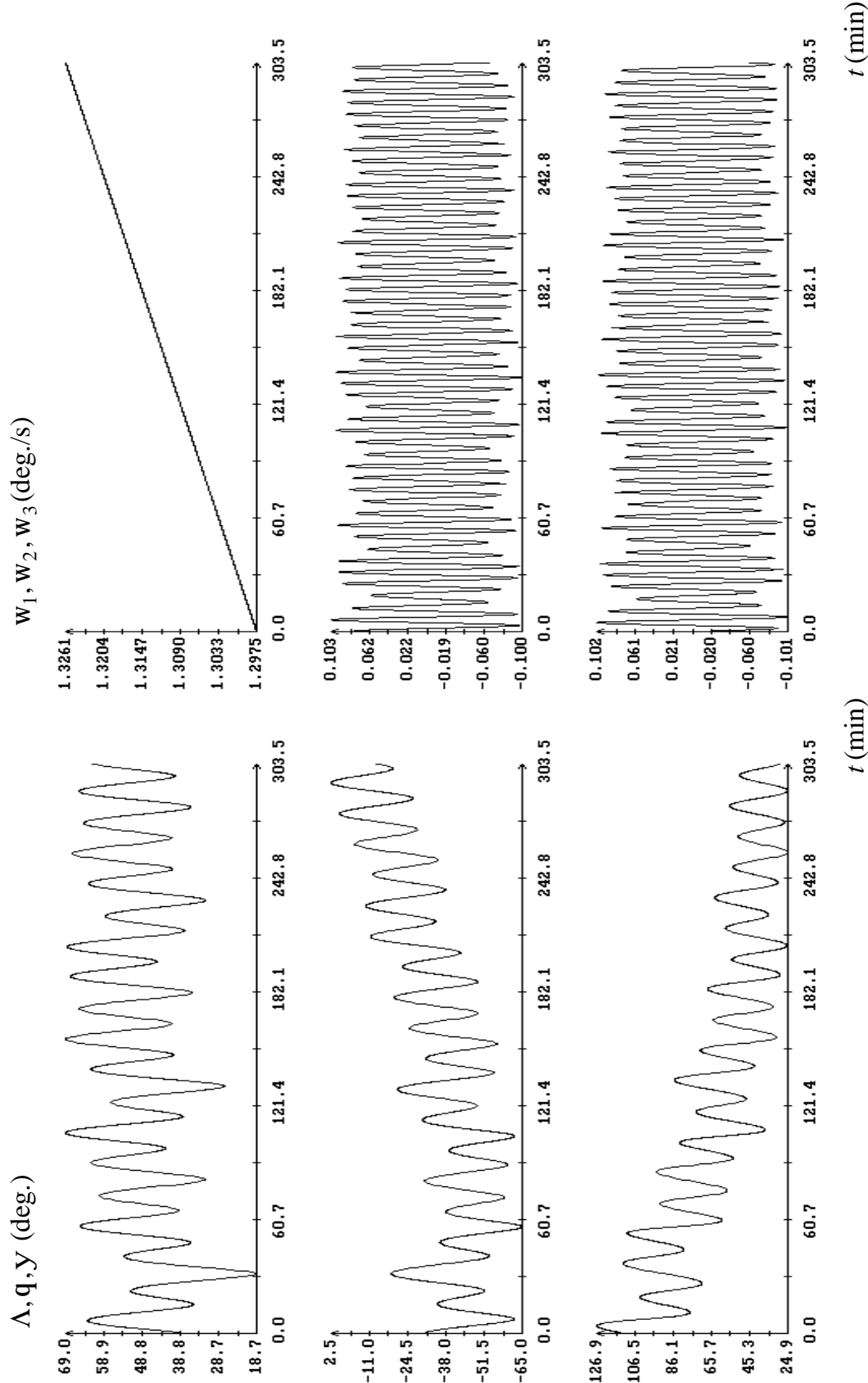
Fig. 7. The motion in interval 10. The instant $t = 0$ corresponds to $t_0 + t$, $t_0 = 08{:}30{:}00$ UTC 13.06.2005, $t = 127.2\,\mathrm{s}$, $s_t = 8.6\,\mathrm{s}$, $s_b = 1.456 \cdot 10^{-6}\,\mathrm{m/s}^2$.

Fig. 8. The acceleration in interval 10. The instant $t = 0$ corresponds to $t_0 + t$, $t_0 = 08{:}30{:}00$ UTC 13.06.2005, $t = 127.2$s, $s_t = 8.6$s, $s_b = 1.456 \cdot 10^{-6}$ m/s^2

26

Λ, q, y (deg.)

w_1, w_2, w_3 (deg./s)

t (min)

t (min)
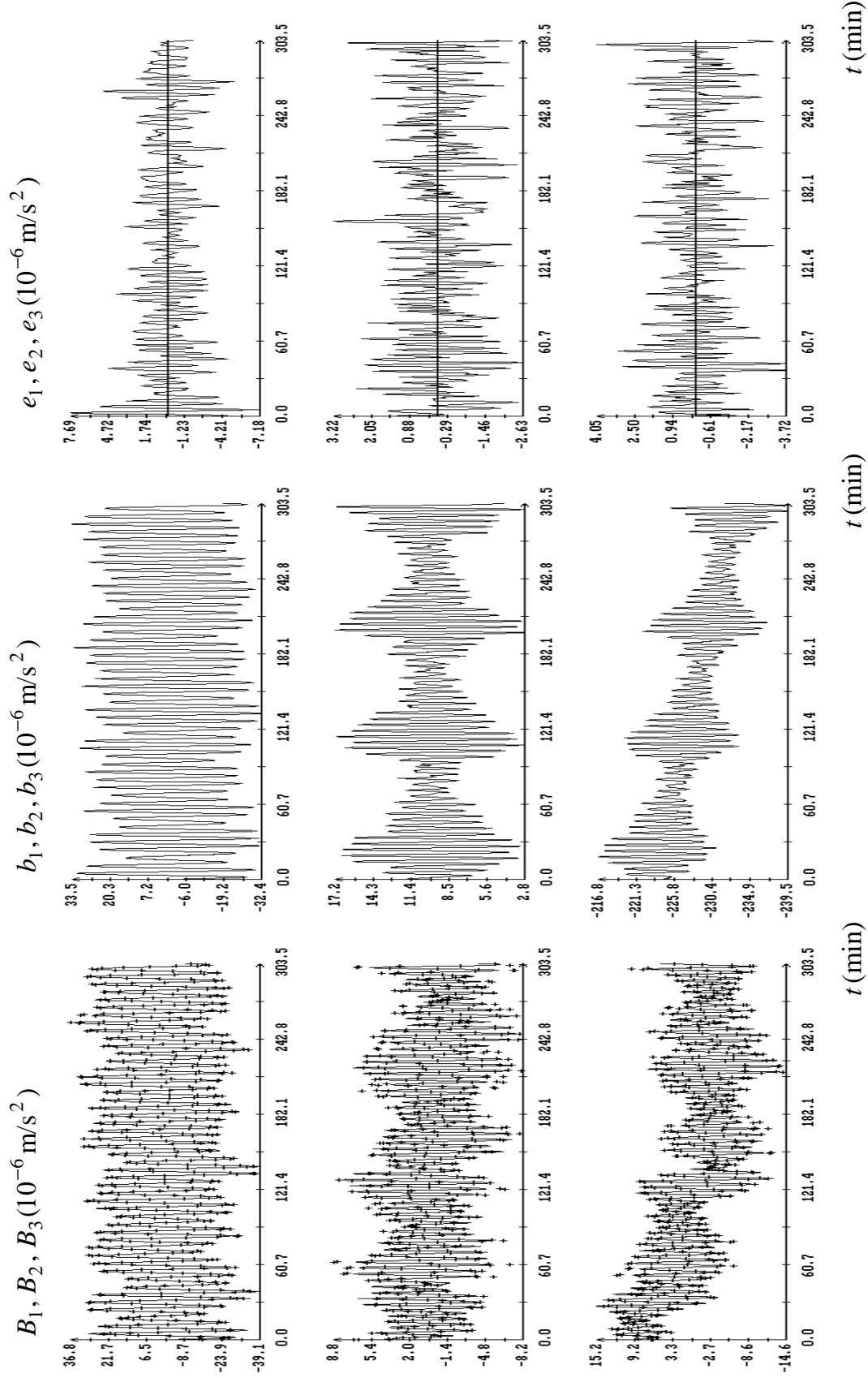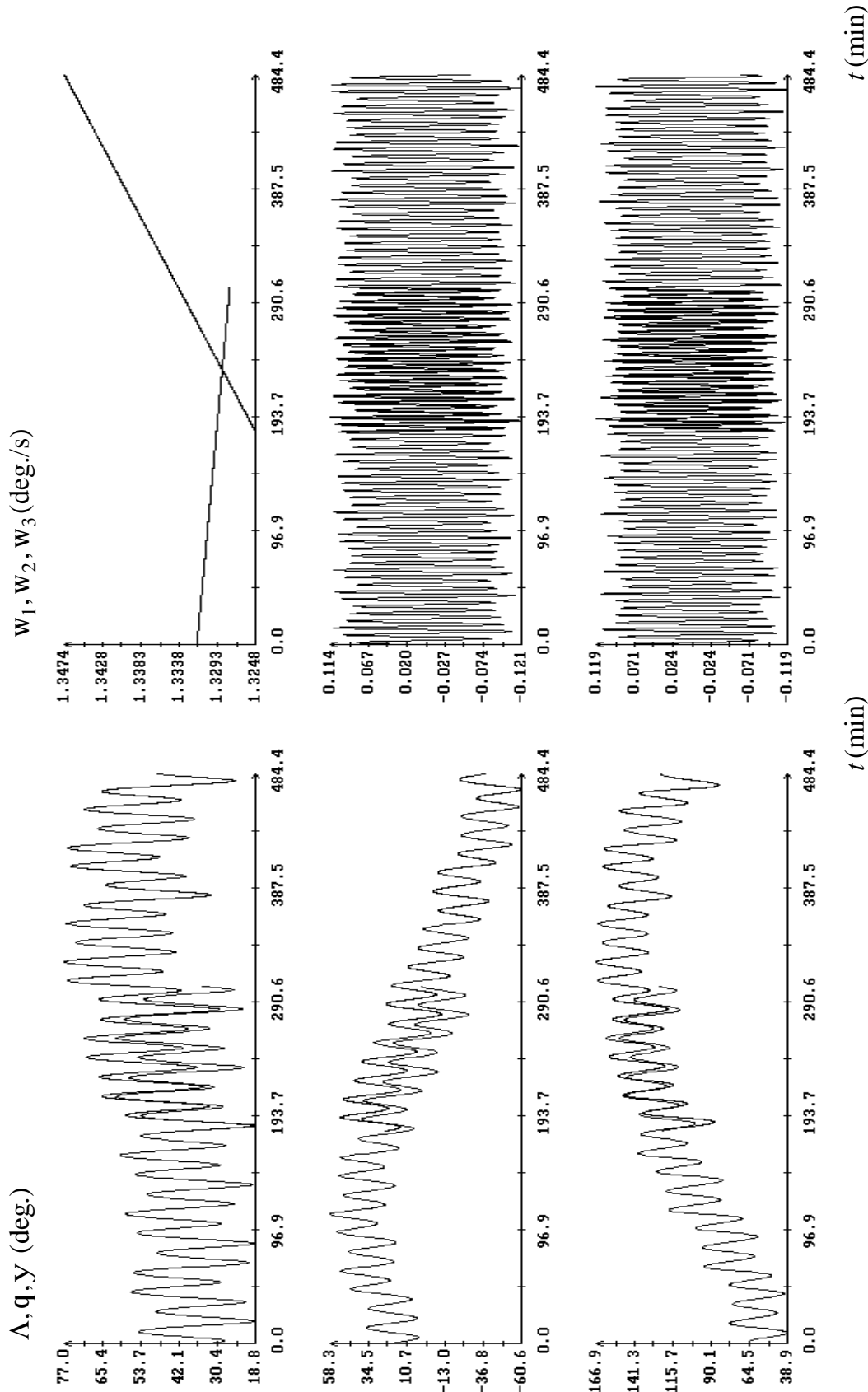
Fig. 9. The motion reconstructions in overlapping intervals 11 and 12 (see Figs. 10, 11). The instant $t = 0$ corresponds to $t_0 + t$, $t_0 = 08{:}30{:}00$ UTC 14.06.2005, t = −84.8s.
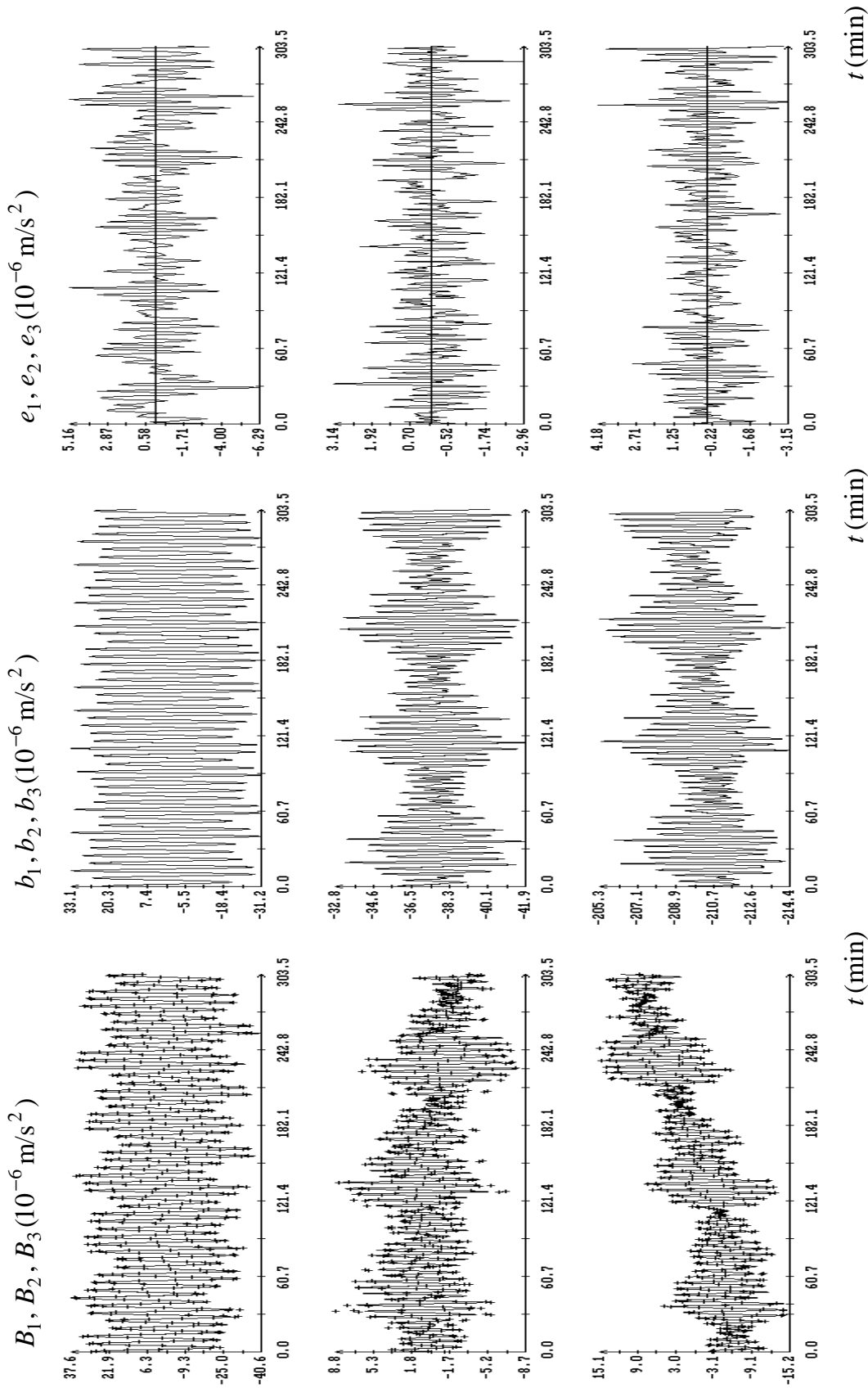
Fig. 10. The acceleration in interval 11. The instant $t = 0$ corresponds to $t_0 + \text{t}$, $t_0 = 08\!:\!30\!:\!00$ UTC 14.06.2005, $\text{t} = -84.8\,\text{s}$, $\text{s}_\text{t} = 11.7\,\text{s}$, $\text{s}_b = 1.390 \cdot 10^{-6}\,\text{m/s}^2$.

28
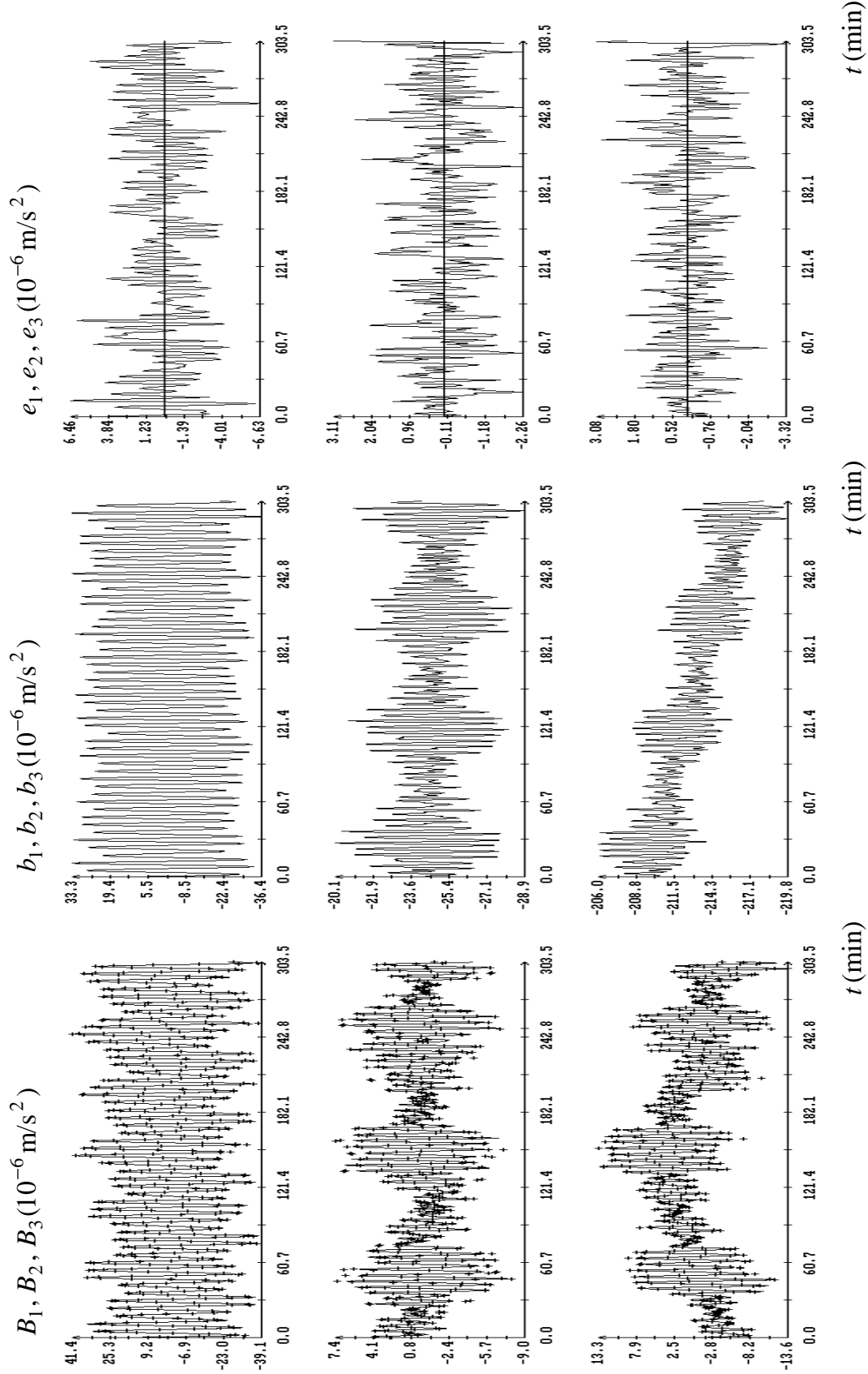
Fig. 11. The acceleration in interval 12. The instant $t = 0$ corresponds to $t_0 + \mathrm{t}$, $t_0 = 11{:}30{:}00$ UTC 14.06.2005, $\mathrm{t} = -3.3\mathrm{s}$, $\mathrm{s_t} = 10.4\mathrm{s}$, $\mathrm{s}_b = 1.495 \cdot 10^{-6}\,\mathrm{m/s}^2$.
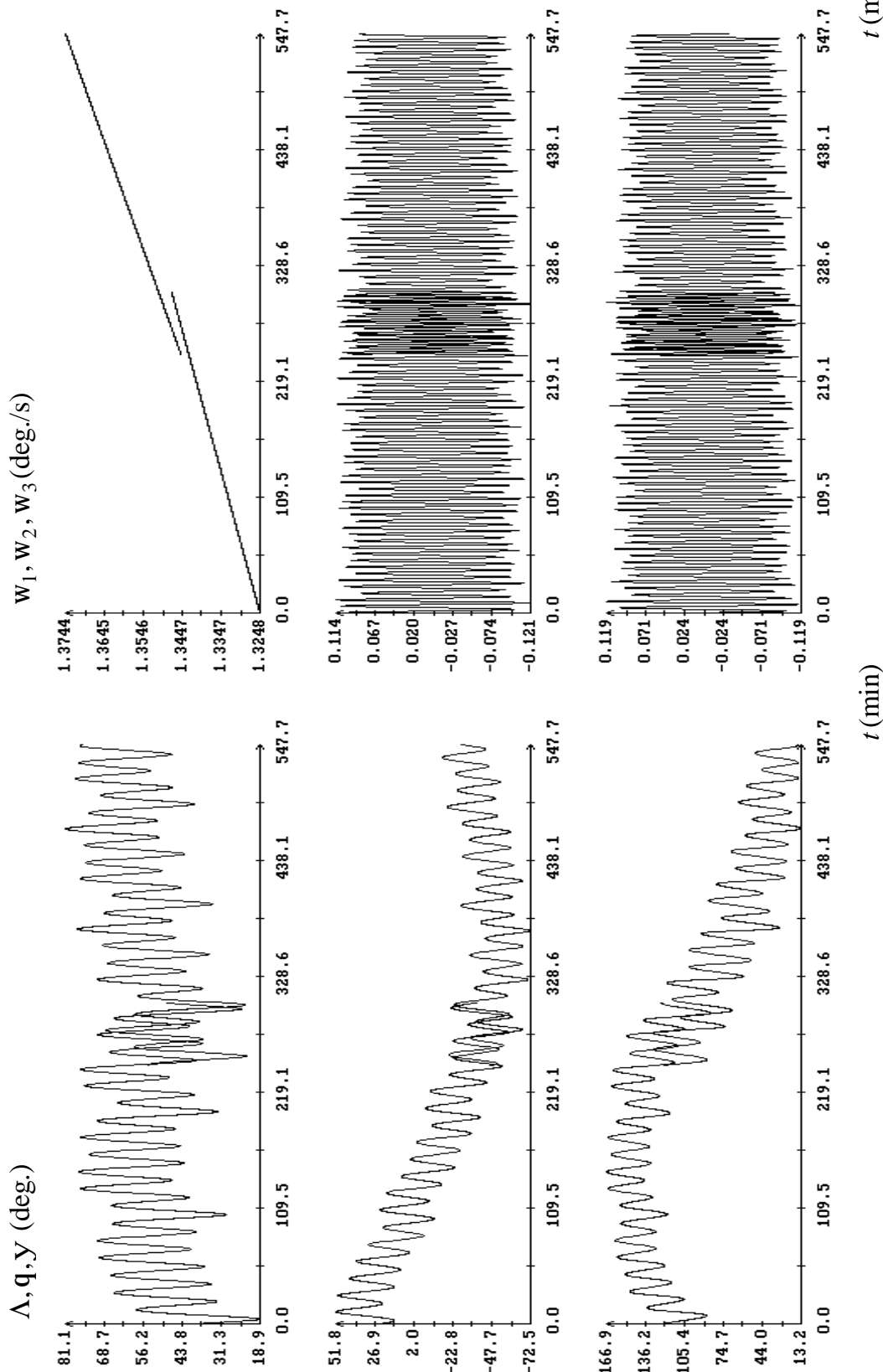
Fig. 12. The motion reconstructions in overlapping intervals 12 and 13 (see Figs. 11, 13). The instant $t = 0$ corresponds to $t_0 + t$, $t_0 = 11:30:00$ UTC 14.06.2005, $t = -3.3$s.
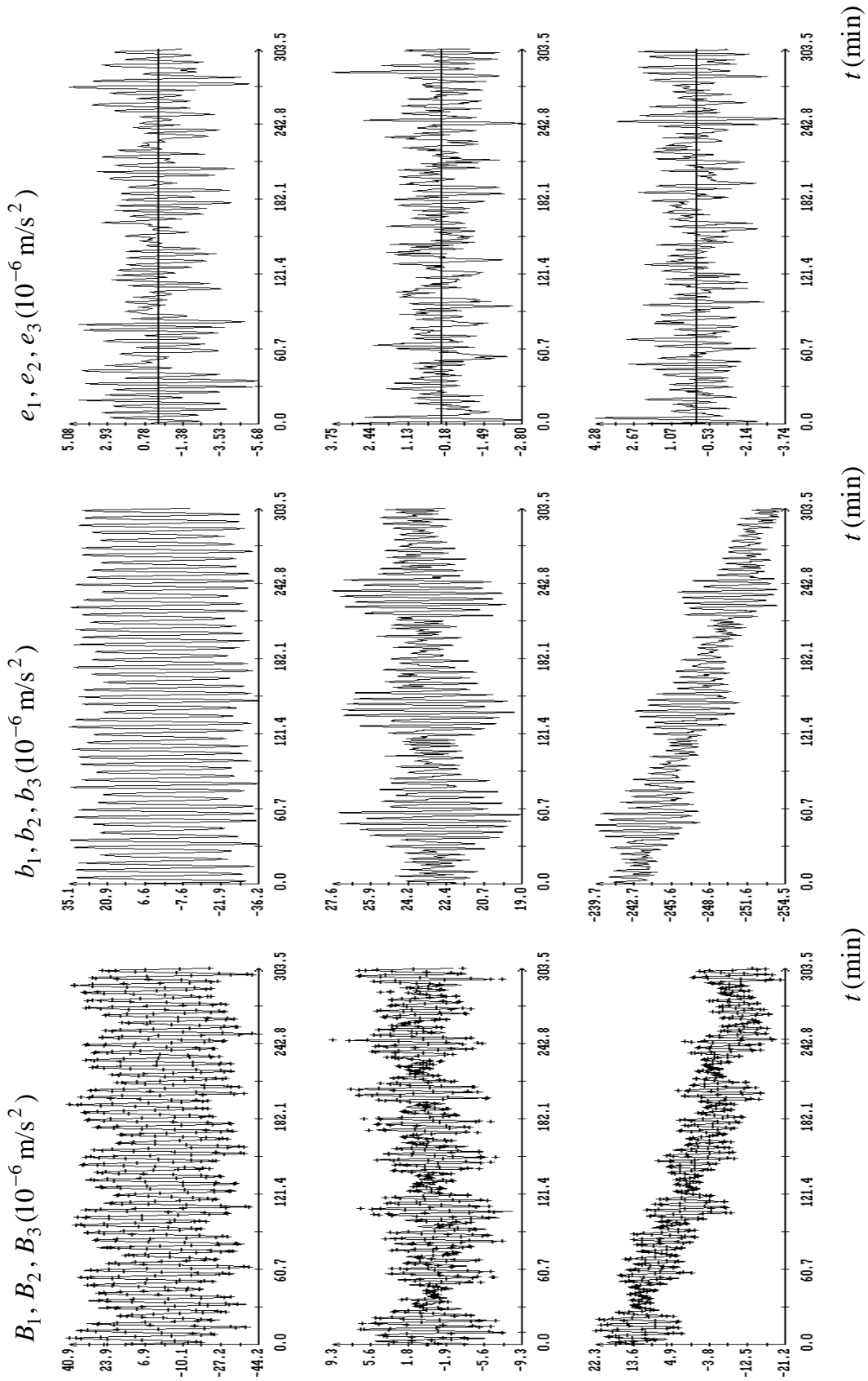
Fig. 13. The acceleration in interval 13. The instant $t = 0$ corresponds to $t_0 + t$, $t_0 = 15:30:00$ UTC 14.06.2005, $t = 216.6$ s, $s_t = 9.6$ s, $s_b = 1.446 \cdot 10^{-6}$ m/s^2.

31